

N 7 1 - 2 4 6 2 6

NASA TECHNICAL
MEMORANDUM

NASA TM X-64586

CASE FILE
COPY

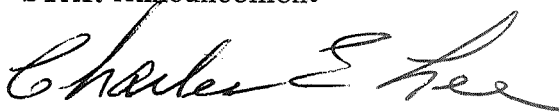
SINGLE-AXIS REFERENCE STRAPDOWN INERTIAL
MEASURING UNIT

By Charles E. Lee
Astrionics Laboratory

March 1, 1971

NASA

*George C. Marshall Space Flight Center
Marshall Space Flight Center, Alabama*

1. REPORT NO. NASA TM X-64586		2. GOVERNMENT ACCESSION NO.		3. RECIPIENT'S CATALOG NO.	
4. TITLE AND SUBTITLE Single-Axis Reference Strapdown Inertial Measuring Unit				5. REPORT DATE March 1, 1971	
				6. PERFORMING ORGANIZATION CODE	
7. AUTHOR (S) Charles E. Lee				8. PERFORMING ORGANIZATION REPORT #	
9. PERFORMING ORGANIZATION NAME AND ADDRESS George C. Marshall Space Flight Center Marshall Space Flight Center, Alabama 35812				10. WORK UNIT NO.	
				11. CONTRACT OR GRANT NO.	
				13. TYPE OF REPORT & PERIOD COVERED Technical Memorandum	
12. SPONSORING AGENCY NAME AND ADDRESS National Aeronautics and Space Administration Washington, D. C. 20546				14. SPONSORING AGENCY CODE	
15. SUPPLEMENTARY NOTES Prepared by Astrionics Laboratory, Science and Engineering					
16. ABSTRACT <p>In-house programs at the Marshall Space Flight Center (MSFC) include design, development, and test of single-axis reference (SAR) strapdown inertial measurement units (IMUs). This effort is described, and the theory and operation of the SAR IMU are presented. Designs and testing of the IMU SARs and accelerometers are discussed. Laboratory, sled, and mobile tests of the IMU system (including the computer) are outlined. Future plans, which include design, development, and testing dodecahedron SAR strapdown IMUs and new gyro concepts for possible application on the space shuttle vehicle, are delineated.</p> <p style="text-align: center;">EDITOR'S NOTE</p> <p>Use of trade names or names of manufacturers in this report does not constitute an official endorsement of such products or manufacturers, either expressed or implied, by the National Aeronautics and Space Administration or any other agency of the United States government.</p>					
17. KEY WORDS Strapdown Inertial measurement unit Single-axis reference Dodecahedron			18. DISTRIBUTION STATEMENT STAR Announcement 		
19. SECURITY CLASSIF. (of this report) Unclassified		20. SECURITY CLASSIF. (of this page) Unclassified		21. NO. OF PAGES 55	22. PRICE \$3.00

ACKNOWLEDGMENTS

The author wishes to express his appreciation to Mr. R. Taylor of the Bendix Corporation, to the personnel of the Astrionics Laboratory's Guidance and Control Division, and to Messrs. T. Gismondi and T. Armstrong of the Space Support Division of Sperry Rand Corporation for their contributions.

TABLE OF CONTENTS

	Page
SUMMARY	1
INTRODUCTION.	1
SAR THEORY AND OPERATION	4
Description of Sensors	4
SAR Formulation and Mechanization	4
SAR and Single-Axis Rate Gyro Comparison	7
Servo Design	10
SD-53 COMPONENT DESIGN AND TEST	13
AB-5 SAR Gyro	13
AMAB-3 Pendulous Integrating Gyro Accelerometer (PIGA)	16
SD-53 TEST PROGRAMS	19
Laboratory Calibration	19
Sled Test	21
Mobile Test.	25
FUTURE PLANS AND PROGRAMS	30
Dodecahedron SAR Strapdown IMU and Computer	30
New Gyro Considerations.	35
CONCLUSION	38
APPENDIX. THE EVENT LOG, COORDINATE DESCRIPTION, AND DRIFT RATE COMPUTATIONS FOR COMPUTER REDUCTION	39

LIST OF ILLUSTRATIONS

Figure	Title	Page
1.	SD-53 strapdown platform	3
2.	SAR mechanization	5
3.	SAR mechanization analog diagram	7
4.	Strapdown single-axis rate gyro mechanization analog diagram	8
5.	SAR servoloop diagram	12
6.	AB-5 SAR gyro	14
7.	Pendulous integrating gyro accelerometer	17
8.	SD-53 installation in the sled	23
9.	Sled test vehicle.	24
10.	Test truck installation.	25
11.	SD-53 alignment in test truck.	28
12.	Breadboard SAR strapdown IMU	31
13.	DDH-MKI SAR strapdown IMU	32
14.	Liquid bearing gyro: LB-5	36
15.	Single-axis ring laser gyro	37
A-1.	Simplified data reduction flow.	42

LIST OF TABLES

Table	Title	Page
1.	Minimum Quantization Level	9
2.	Summary of SD-53 Strapdown Sled Test	22
3.	CTMC Functional Characteristics	26
4.	Determinant Error	29
5.	Inertial Axes Drift	30
6.	Change In Drift Rate	30
7.	Honeywell DDP-516 Computer Characteristics	34
A-1.	SD-53/CTMC Van Test: November 13, 1970, Event Log	39
A-2.	SD-53/CTMC Van Test: November 19, 1970, Event Log	40
A-3.	SD-53/CTMC Van Test: November 20, 1970, Event Log	41
A-4.	Van Test Coordinates Frames	43

DEFINITION OF SYMBOLS

<u>Symbol</u>	<u>Definition</u>
B sign ($\dot{\phi}$)	coulomb friction term where sign ($\dot{\phi}$) is +1 for positive rate ($\dot{\phi}$) and -1 for negative rate ($\dot{\phi}$)
$C\phi, S\phi$	cosine and sine of the angle ϕ
D	viscous damping coefficient
$f(\theta)$	servo transfer function
h	gyro spin momentum about the spin reference axis
I_1, I_3	moments of inertia of the gyro float about the output and input axes, respectively
J_3	moment of inertia of the single-axis reference shaft about the input axis
K	gain factor
T_s	strobe time
$\Delta\phi$	small shaft angle
θ	gyro precession angle
ϕ	single-axis reference shaft angle
$\dot{\phi}$	single-axis reference shaft rate
$\ddot{\phi}$	single-axis reference shaft acceleration
$\omega_1, \omega_2, \omega_3$	body rates about the output, spin reference, and input axes, respectively

SINGLE-AXIS REFERENCE STRAPDOWN INERTIAL MEASUREMENT UNIT

SUMMARY

In-house programs at the Marshall Space Flight Center (MSFC) include design, development, and test of single-axis reference (SAR) strapdown inertial measurement units (IMUs). This effort is described, and the theory and operation of the SAR IMU are presented. Designs and testing of the IMU SARs and accelerometers are discussed. Laboratory, sled, and mobile tests of the IMU system (including the computer) are outlined. Future plans, which include design, development, and testing dodecahedron SAR strapdown IMUs and new gyro concepts for possible application on the space shuttle vehicle, are delineated.

INTRODUCTION

The Marshall Space Flight Center is very active in the field of space vehicle inertial navigation. Many gimballed stabilizer platform systems have been designed, fabricated, and tested by MSFC and its contractors. These systems have successfully flown on such space vehicles as the Redstone, Jupiter, Pershing, and Saturn.

Experience in inertial systems at MSFC dates back to the early 1950s in this country and to the 1930s with the association of Dr. Wernher von Braun in Germany. One of the first systems refined at Huntsville, Alabama, was the LEV-3. This was an inertial attitude reference system with velocity cut-off pendulous integrating gyro accelerometers (PIGAs). It was essentially a strapdown platform consisting of two two-degrees-of-freedom gyros for control of the pitch, yaw, and roll axes. This system was used in 1961 in the guidance of the Mercury-Redstone vehicle that placed the first astronaut (Alan Shepard) into space.

It became apparent in the early 1960s that a strapdown type of inertial navigation would be very attractive for space vehicle application. This is evident because of the advancement in computer technology, the giant strides made in the electronics field, and the ease in achieving redundancy management.

The first strapdown designed, developed, and fabricated at MSFC was designated the SD-53 (Fig. 1). It was designed with Saturn ST124 gimbaled-type components, e. g., AB-5 (5-cm wheel diameter) air bearing gyros and AB-3 PIGA (3-cm wheel diameter). The AB-5 gyros were arranged in an SAR or a single-axis platform (SAP) configuration to perform the angular rate sensing. The SARs utilize 18-bit encoders and are servo controlled with dc torquers.

As theory will indicate, the SAR strapdown IMU has certain advantages over the conventional strapdown for applications to the space shuttle type of vehicle. Some of these advantages are as follows.

1. High-vibration rates are easily detected.
2. The requirement for a wide dynamic range torquer is eliminated.
3. The encoder digital outputs on the SAR are equivalent to torquer pulses in a conventional pulse rebalance gyro control loop.
4. Failure detection and redundancy management are easily implemented.

The SD-53 strapdown was developed primarily to obtain more information on strapdown behavior in a space booster environment. It was planned to be an experiment on a future Saturn launch vehicle. An interface computer was also designed and developed at MSFC and was designated the coordinate transformation matrix computer (CTMC). It was designed to function with the existing Saturn digital flight computer. Because of limited funds and other projects with higher priority, this program was not concluded. However, this paper will describe the SD-53 IMU, its component, and system testing.

Future programs include investigation of redundant IMUs. One such concept is the dodecahedron SAR IMU. It is now under design and development together with advanced inertial sensors, high-density integrated circuit electronics for servoloops, control logic, failure detection, and fault isolation.

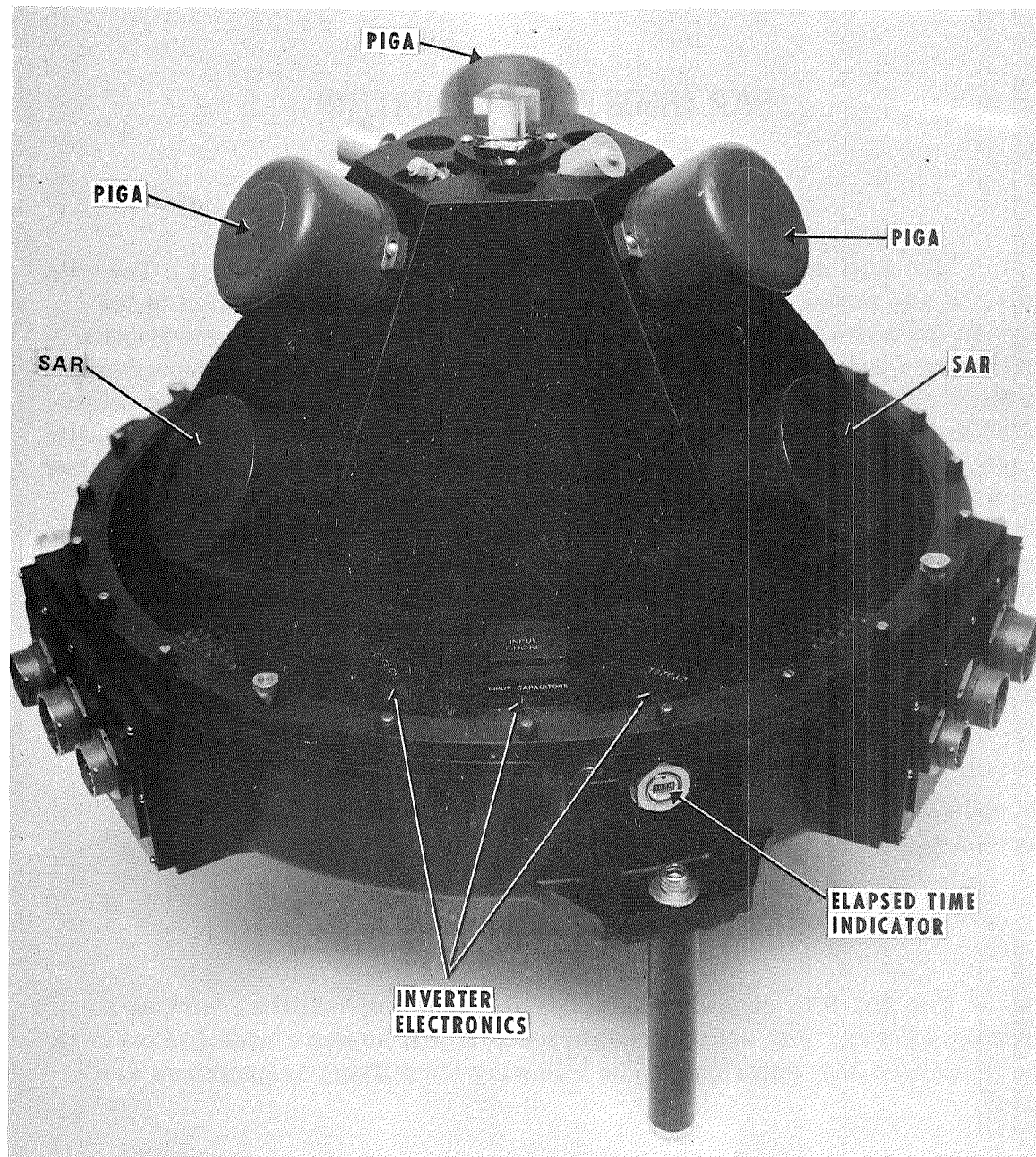


Figure 1. SD-53 strapdown platform.

SAR THEORY AND OPERATION

Description of Sensors

The SAR mechanization is shown schematically in Figure 2. The rate gyro, G, and signal generator, SG, assembly (no torquer is coupled to the float in the SAR) is mounted on a shaft, S, that, except for coulomb friction and viscous damping of the support bearings, is free to rotate independently of the base. The friction and viscous forces, resulting when the base rotates, exert torques on the shaft that causes gyro precession. The gyro precession angle, θ , is sensed by the signal generator. The resulting error signal, after amplification and compensation, drives the torquer. Thus, the shaft rate relative to the base, $\dot{\phi}$, is equal to the negative of the base inertial rate about the shaft axis, ω_3 . The shaft angle about the base, ϕ , equals the negative of the integral of ω_3 . In this application, increments of ϕ are sensed by an incremental optical encoder. The size of each increment corresponds to the quantization level of the least significant bit of the encoder. The ϕ increments are summed by an asynchronous up/down counter as they occur.

The counter is strobed (read + cleared) at a time interval T_s and its contents are obtained as $\Delta\phi$. It should be noted that the gyro precession angle is always very nearly zero in the SAR system.

SAR Formulation and Mechanization

The full-SAR equations have been formulated, including various error-inducing effects. For the present purposes it will be more useful to examine the simplified SAR equations. The following simplifying assumptions are made.

1. No center-of-mass offsets exist.
2. No anisoelastic effects exist.
3. No anisoinertia effects exist.
4. The gyro precession angle, θ , and the shaft rate, $\dot{\theta}$, are negligible because of viscous damping.
5. The base inertial rate, $\dot{\omega}$, is very small.

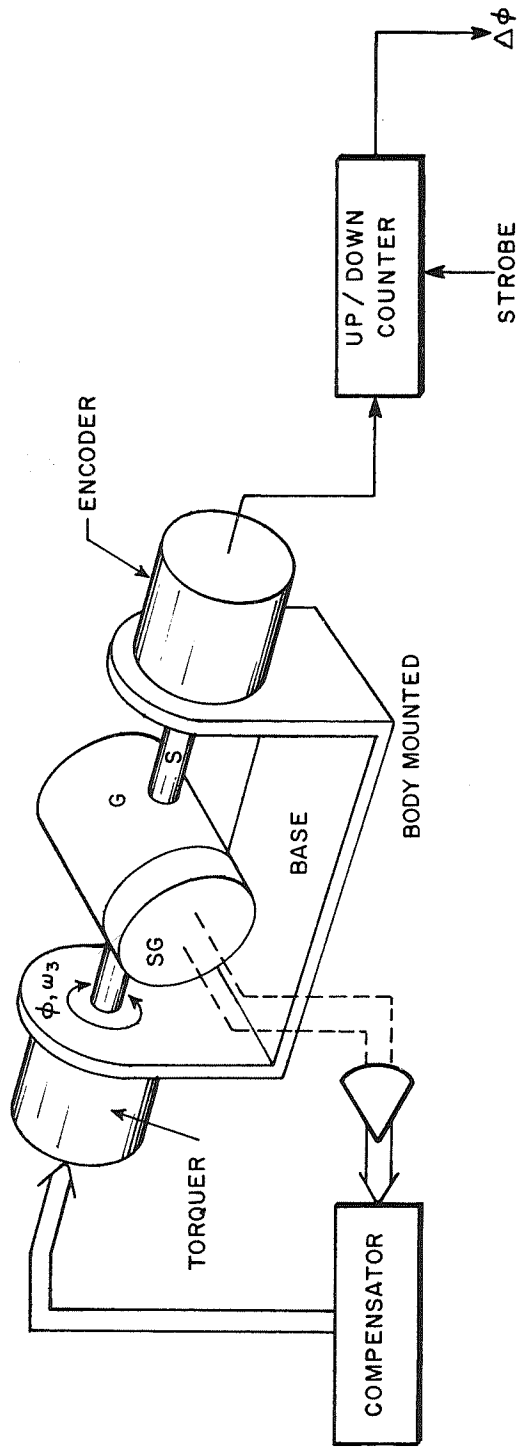


Figure 2. SAR mechanization.

These assumptions, together with the culmination of certain higher order terms, lead to

$$\begin{pmatrix} 0 \\ 0 \\ J_3 \ddot{\phi} \end{pmatrix} + \begin{pmatrix} -h(\omega_3 + \dot{\phi}) \\ 0 \\ h(\omega_1 C\phi + \omega_2 S\phi) \end{pmatrix} + \begin{pmatrix} I_1 \ddot{\theta} \\ 0 \\ I_3 \ddot{\phi} \end{pmatrix} = \begin{pmatrix} 0 \\ 0 \\ f(\theta) - D\dot{\phi} - B \text{sign}(\dot{\phi}) \end{pmatrix} .$$

By neglecting $h(\omega_1 D\phi + \omega_2 S\phi)$, the disturbance torques caused by rates about the output and spin reference axes yield:

$$h(\omega_3 + \dot{\phi}) = I_1 \ddot{\theta} \quad , \quad (1)$$

$$\ddot{\phi}(I_3 + J_3) = K\theta - D\dot{\phi} \pm B \quad . \quad (2)$$

Eliminating θ between the two equations yields

$$h(\omega_3 + \dot{\phi}) = I_1/K [(J_3 + I_3) \ddot{\ddot{\phi}} + D\ddot{\phi}] \quad .$$

By recalling that

$$K \rightarrow \infty$$

so that

$$\omega_3 \approx -\dot{\phi} \quad ,$$

equation (2) can be written in the form

$$(I_3 + J_3) \dot{\omega}_3 + D\omega_3 + B \text{sign}(\omega_3) \approx K\theta \equiv f_1(\theta) \quad . \quad (3)$$

Under the same assumptions used in the previous analysis, the single-axis rate integrating gyro admits the following equation:

$$\frac{-D\dot{\theta} + f_2(\theta) + I_1 \ddot{\theta}}{h} = \omega_3 \quad (4)$$

The ideal SAR mechanization and the strapdown single-axis rate gyro mechanization are shown in Figures 3 and 4, respectively.

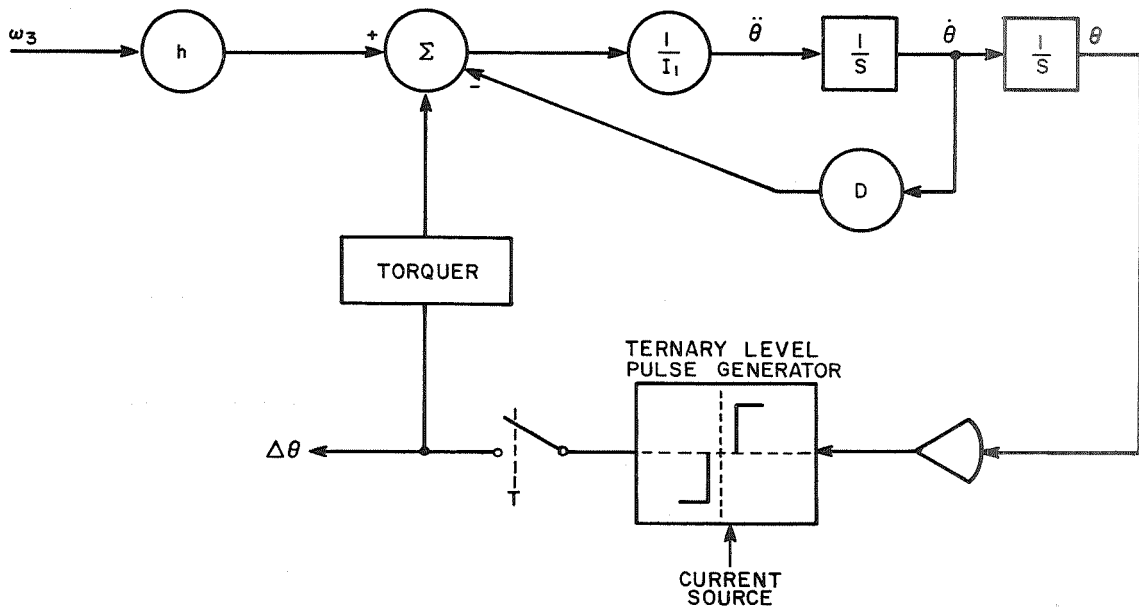


Figure 3. SAR mechanization analog diagram.

SAR and Single-Axis Rate Gyro Comparison

The SAR quantization method is equivalent to the ternary method used in the strapdown single-axis rate gyro mechanization (Fig. 4) if the strobe interval T_s is small enough so that at the most one (+1 or -1 or zero times the minimum quantization unit) pulse is outputted as $\Delta\phi$ during any one internal T_s .

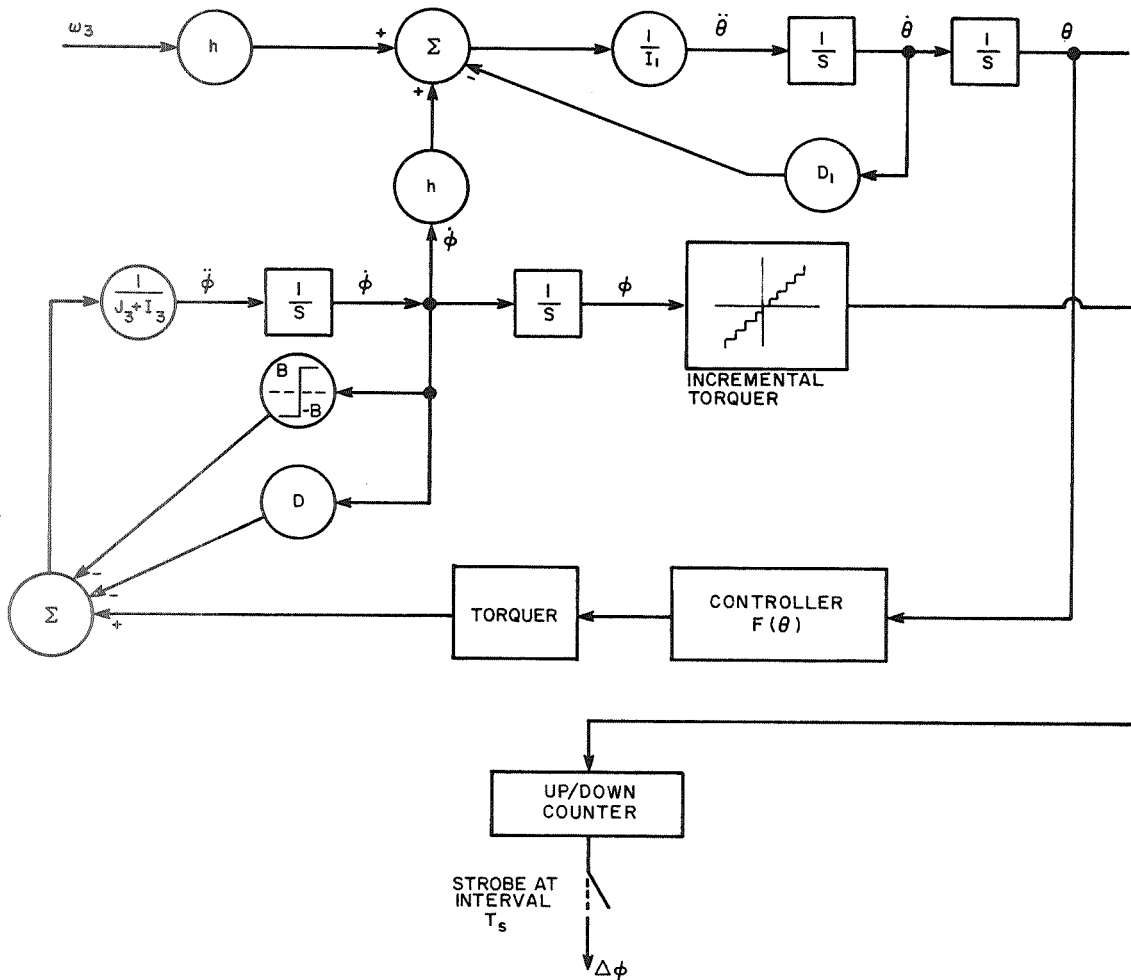


Figure 4. Strapdown single-axis rate gyro mechanization analog diagram.

The SAR accuracy depends on the encoder quantization level (and alignment). The minimum quantization level for 16- through 19-bit encoders is given in Table 1.

The limiting factor for the strapdown single-axis rate gyro is the accuracy with which the current pulses can be generated (plus with which $\Delta\theta$ can be quantized). It is anticipated that the resulting minimum $\Delta\phi$ quantization level of $29 \mu\text{rad}$ will be typical for an actual system application. Thus, an SAR with an 18-bit encoder should provide equal or slightly better minimum quantization level.

TABLE 1. MINIMUM QUANTIZATION LEVEL

Number of Bits in Encoder	Minimum Quantization Level (μrad)
16	96
17	48
18	24
19	12

If an SAR is required to operate with input rates up to 1 rad/s, a typical requirement places stringent requirements on the servo design; however, no significant difficulties in achieving the desired rate-capability are apparent.

In the event that a similar requirement is placed on the strapdown single-axis rate gyro system, similar constraints will be placed on the torquer, current source, ternary pulse generator, etc. Now, however, a problem arises in generating the precise current pulses (each representing $\approx 29 \mu\text{rad}$) at a rate ($\approx 35 \text{ kHz}$) corresponding to the required input rate. It is necessary to have two discrete $\Delta\theta$ quantization levels (coarse and fine) to achieve the desired rate capability (1 rad/s). The requirement that the system operate accurately at two different quantization levels would place more stringent requirements on the already complicated torquer and current supply.

With the SAR system, a proper servo design will assure that

$$\Delta\phi = \int_0^T \omega_3 dt$$

for some range of ω_3 . With the system shown in Figure 3, note that

$$\Delta\theta \neq \int_0^T \omega_3 dt$$

but rather

$$F_T(\Delta\theta) = - \int_0^T \omega_3 dt \quad ,$$

where F_T is the very complex torquer open-loop transfer function. In general, F_T is not constant because of such factors as aging, temperature effects, and nonlinear torque coupling with the float.

In the SAR system, the lack of direct coupling between the torquer and the gyro float eliminates a number of problems, which are listed below.

1. The requirement for an exceptionally accurate ternary level current pulse source is eliminated.
2. The requirement that the torquer and current supply be able to operate at distinct (coarse and fine) levels is removed.
3. The possibility of torquer to signal generator coupling is eliminated.
4. The problems associated with thermal control of the torquer in the presence of varying power dissipation levels (i. e. , varying frequency of non-zero pulses) are removed.
5. The need for a very accurate torquer with an extraordinarily constant scale factor is relaxed.
6. The detrimental effects of torquer nonlinearity are eliminated.

Servo Design

The fundamental design requirement is that

$$\dot{\phi} \cong - \omega_3 \quad ,$$

for arbitrary ω_3 within boundary specifications on ω_3 max, ω_3 min, $\dot{\omega}_3$ max. The effect of angular rates about the other axes ω_1 , ω_2 is to cause a disturbance torque $h(\omega_1 C\phi + \omega_2 S\phi)$ at the table. Proper design must minimize errors in $\dot{\phi}$ caused by this disturbance.

An outline of the servoloop is shown in Figure 5. The gyro output signal demodulator has been omitted for convenience.

The servo is type 1, with no integrator in the compensator; if non-linearity effects and disturbances are neglected, ϕ can equal exactly constant values of ω_3 .

It is customary, however, to add an electronic integrator to the compensator resulting in a type 2 servo. With the added integrator, the servo can follow a slowly changing ω_3 more accurately and further reduce errors caused by disturbances at the table. In a typical servo design, a loop bandwidth of 100 Hz has been obtained.

The preceding discussion has been based on considerable simplification of the gyro dynamics involved. The major assumptions are:

1. Perfect alignment.
2. Ideal instrument construction.
3. Dynamic environment consisting only of a constant input rate about the instrument input axis.

A detailed analysis to determine the relative significance of potential error sources is underway at MSFC. A more complex equation can be written to represent the complete SAR dynamical behavior and includes such effects as:

1. Center-of-mass effects of both float and outer gimbal.
2. Anisoelastic effects.
3. Anisoinertia effects.
4. Misalignments.
5. Angular rates and accelerations about all three axes.

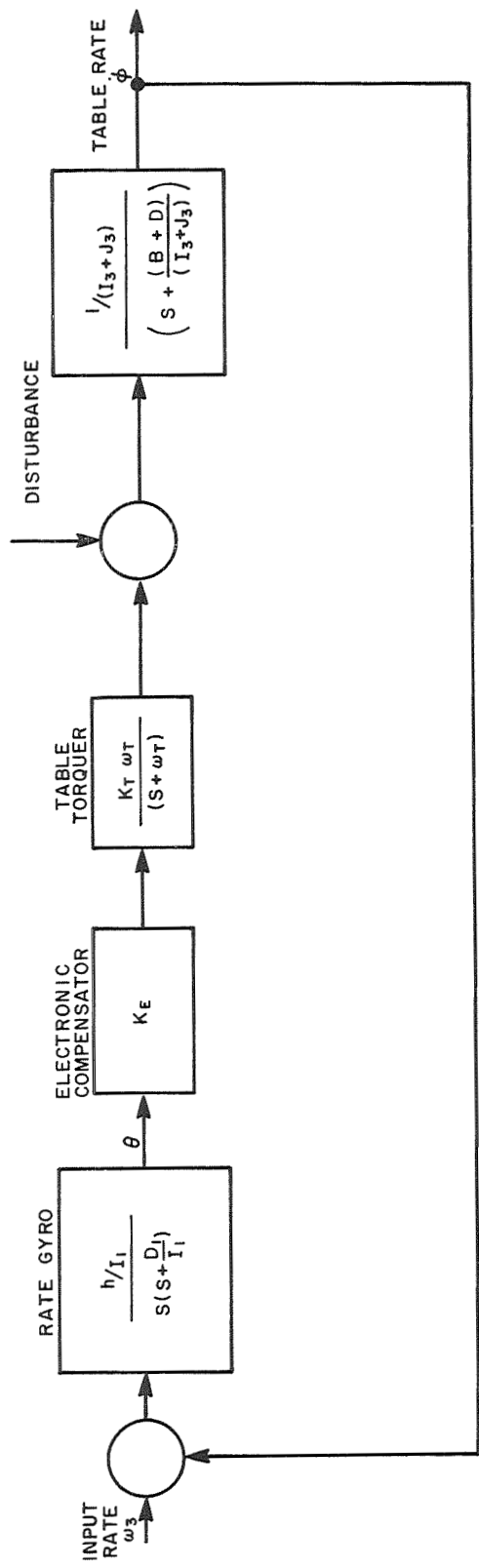


Figure 5. SAR servoloop diagram.

The relative importance of each of these effects can be determined by means of computer simulations. The objective of these studies is to determine the important design requirements for the rate gyro and other components and then evaluate overall system accuracy for a particular mission or application.

SD-53 COMPONENT DESIGN AND TEST

AB-5 SAR Gyro

Description and Design. The AB-5 SAR shown in Figure 6 provides inertial reference position information about an axis perpendicular to its mounting plane. The instrument assembly consists of the following major items or subassemblies: output encoder, housing, servoed axis dc torquer, intermediate assembly, and servo-electronics.

At the time of its conception and design (about 1964), the AB-5 SAR was considered a preliminary breadboard package. For all purposes, it is still that. Smaller packages have been considered and are in the layout stage, but this instrument is still the only one of its type. The initial concept was to build an SAR package around the Saturn K8-AB-5 gyro, and this is how the size was dictated. The inner gimbal gyro assembly and the gyro output axis gas bearing are essentially the Saturn gyro design of the ST124 Saturn IB configuration.

The piece parts for these instruments were designed and manufactured at MSFC except for items such as the dc torque motor, the encoder, and those that are interchangeable with the Saturn gyro. Six sets of parts were started; five instruments were actually assembled, three for the SD-53 with two spares. The instruments were assembled and tested as components before mounting in the system. Tests were designed to determine the misalignment errors of the package and the conventional performance parameters such as g sensitive and non-g sensitive characteristics. The gyro gimbal assemblies used in these instruments were more or less "culls" from the Saturn IB program. All had either marginal or unsatisfactory performance characteristics; but they were available, and no great emphasis was being placed on performance.

The encoder used as the position output device on the AB-5 SAR was purchased from Dynamic Research Corporation. It is an incremental encoder with an output of 2×10^{18} bits dual channel (sine and cosine) and an extra channel for a zero reference, single-pulse output. The encoder is built around a set

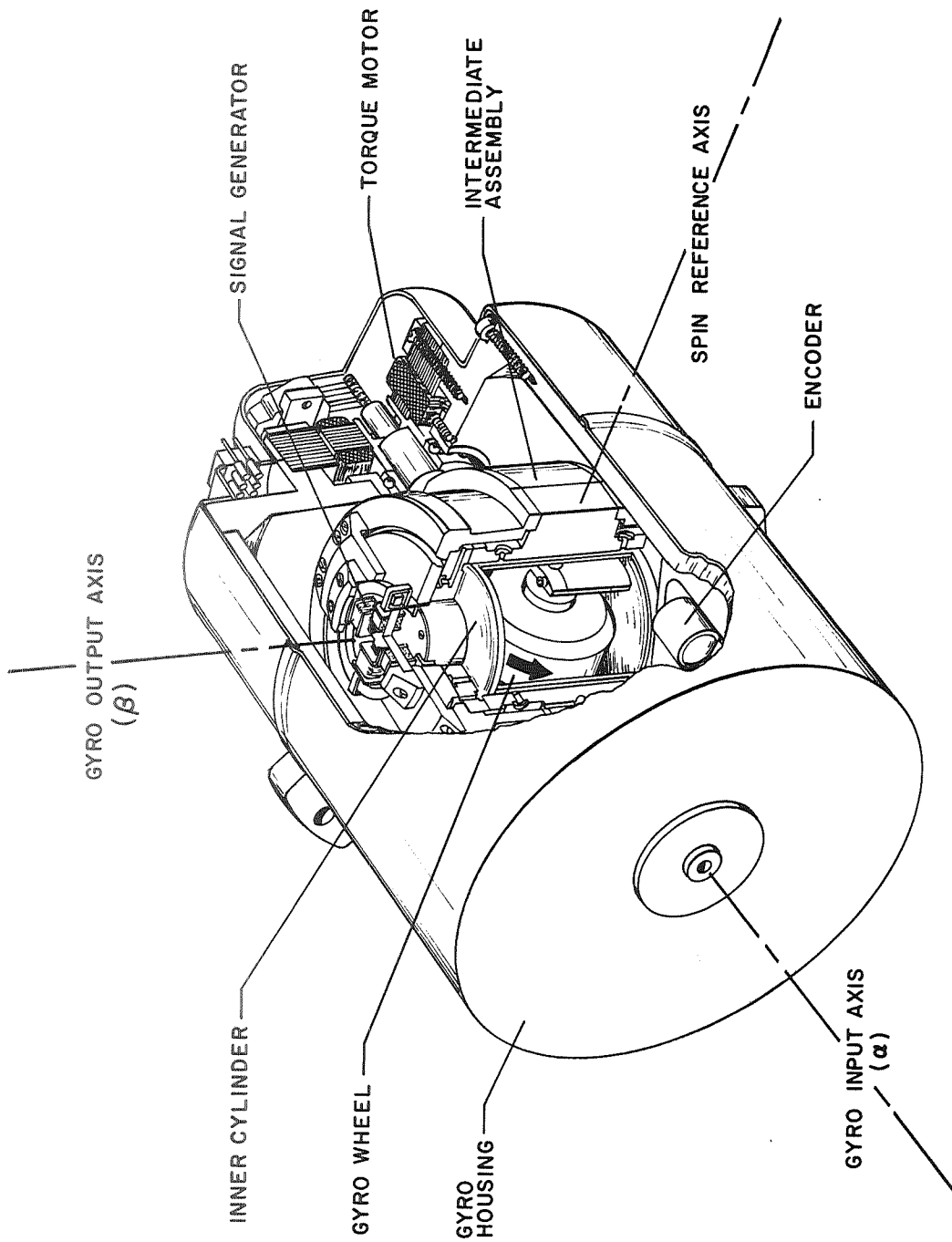


Figure 6. AB-5 SAR gyro.

of preloaded precision bearings mounted in a beryllium housing. Linearity and accuracy tests were performed on the encoders before they were assembled into the SAR. The housing bearing and rotating disk mounting hub of the encoders were assembled and aligned to the encoder. This permitted precision alignment and fitting to the SAR housing.

The housing for the SAR essentially provided the servoed axis bearing support system, the servo torquer mounting, and the precision alignment of this servoed axis. The housing was machined from beryllium. Since the servoed axis is supported by a three-bearing system, a preloaded set in the encoder and a single bearing on the other end of the axis precision fits and alignments were critical. It was not possible to assemble the encoder into the SAR housing from piece parts as had been experienced with lower accuracy encoders. For this reason and the requirement for critical alignment of the three bearings, the encoder housings with their preloaded bearing sets selected and installed were fitted to the mating diameter and surfaces of the housing. This permitted line bore finishing of the third bearing bore. The three mounting pads were machined flat and perpendicular to the servoed axis bearing bore. Later, following instrument assembly, these pads were lapped to a perpendicular of less than $\pm 25 \mu\text{rad}$ to the actual servo axis of the instrument. This measurement was performed using optical measuring techniques that incorporated a mirror mounted directly on the end of the servoed axis. Slip-rings and a gas swivel were provided to operate the gyro and gas bearing.

The gas bearing sleeve was designed with the same parameters as the standard K8-AB-5 gyro. Trunnions were provided as integral parts of the sleeve. These trunnions were precisely machined perpendicular to the gas bearing bore. They were all $\pi/2$ rad to the gas bearing within a few microradians. The sleeve of the gas bearing is beryllium; the thrust plates are monel.

The servo pickup and the torquer are assemblies from the Saturn K8 gyros. These are shorted turn-variable reluctance types.

The gas bearing incorporated two rows of 24 feeder orifices, the same as the Saturn K8 gyro. The operating gaps were 17×10^{-4} to 20×10^{-4} cm. The flow requirement at 10 N/cm^2 is 2000 standard cm^3/min . The restrictors used in the feeder orifices of this bearing are the same as those used in the K8 gyro.

The gyro motor gimbal assemblies used in these SAR assemblies were salvaged from the early Saturn V hardware. The motor characteristics are:

26 V, 3 phase, 400 Hz, hysteresis, synchronous, 2.50×10^3 rad/s angular velocity, and an angular momentum of 2×10^3 kg-cm²/s. These gyro motors had monel rotors and endbells with a 52100 steel spin-axis bearing. The gimbal is beryllium.

Laboratory Test. Laboratory performance tests of the SAR instrument assembly were of two general types: tests to determine the normal g and non-g sensitive terms of the gyro assembly and dynamic tests to isolate and determine errors in alignments of the various axes of the instrument. These tests were performed on a Fecker Model 352 gas bearing test table. A mounting bracket was provided on the table top and was precisely aligned optically to the table axis.

A series of standard six-position tests was performed with the instrument accurately positioned relative to local g and azimuth. The instrument servoed axis was precisely defined by a mirror attached to the end of this axis. This accurate position information was necessary to define the misalignment errors in the instrument. Performance of the instrument was determined by using up/down counters on the Theodosyn output. No biasing was incorporated in the instrument so the position information from the encoder was drift angle. During the dynamic tests, extreme accuracy was required in determining the relative position of the SAR to the table axis. For example, if no other error exists in the instrument, a $175\text{-}\mu\text{rad}$ misalignment of the SAR servoed axis to the table axis at $\pi/2$ rad will produce an error of $29\ \mu\text{rad/s}$ in the instrument output with a table rate of 0.17 rad/s. The IA of the gyro was aligned in one plane to the trunnion or servoed axis of the SAR by positioning the null of the servo pickup; in the other plane, the misalignment can only be measured and compensated. The alignment of the mounting plane to the servoed axis cannot be changed; this error must be defined and compensated. This error was less than $25\ \mu\text{rad}$ on all the instruments on the SD-53.

AMAB-3 Pendulous Integrating Gyro Accelerometer (PIGA)

Description and Design. The AMAB-3-K8 is a PIGA used on the ST124-M inertial guidance platform for the Saturn IB and V launch vehicles (Fig. 7). The accelerometer consists of a gyro assembly mounted inside a can or float. The float is suspended inside the measuring head assembly on a gas bearing. A signal generator is mounted on one end of the float, and the gyro motor flexleads are mounted on the other end. The float is physically limited to ± 0.10 -rad rotation about the gyro output axis. The measuring head assembly is free to rotate on ball bearing supports (trunnions) inside the main housing. Sliprings, a dc torque motor, and an optical encoder complete the PIGA assembly.

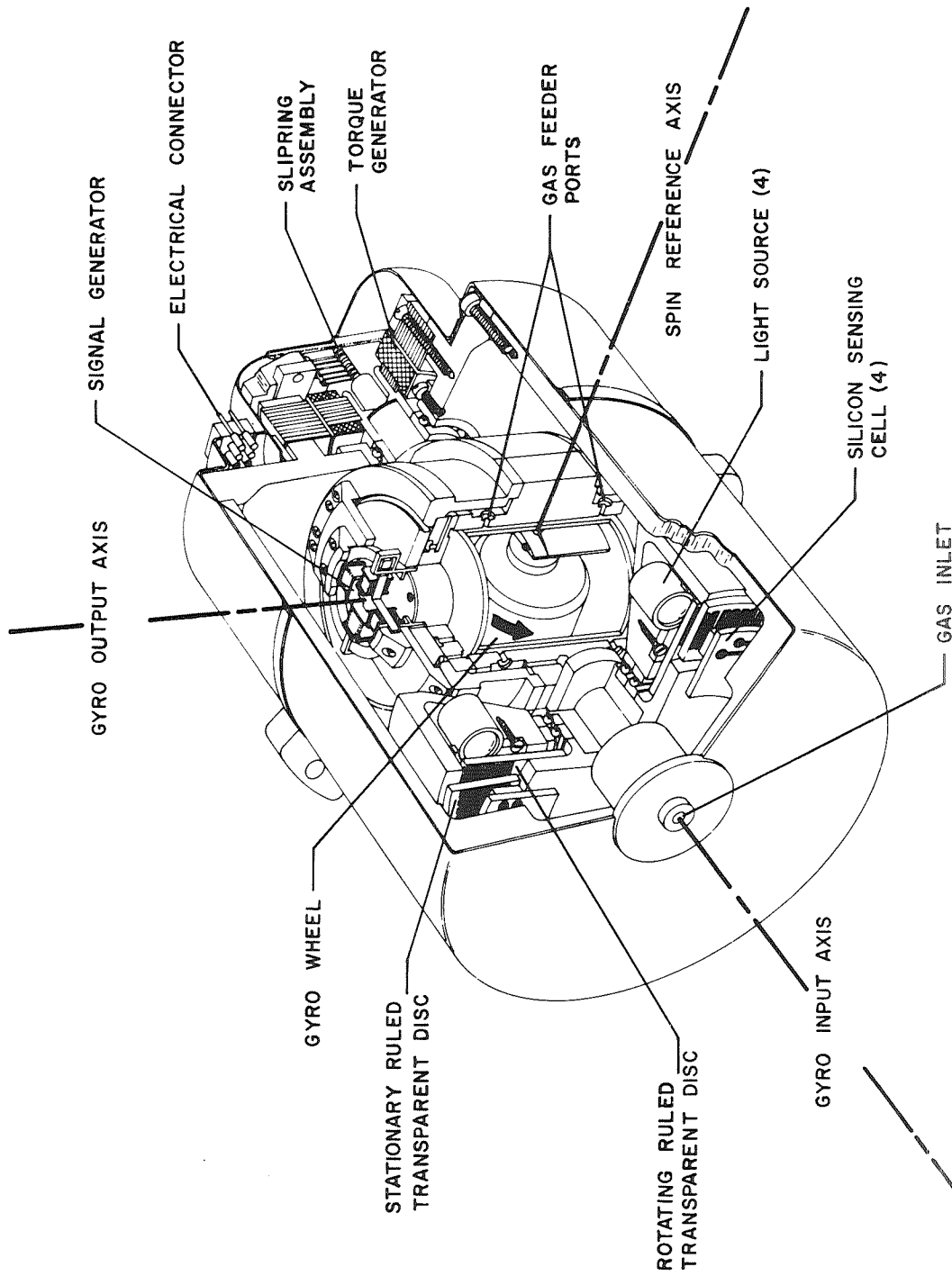


Figure 7. Pendulous integrating gyro accelerometer.

The gyro is mounted inside a beryllium can called the float assembly because it is supported entirely by a gas film 0.0015 to 0.002 cm thick. The motor has a momentum of $100 \text{ kg-cm}^2/\text{s}$ with a wheel speed of $1.25 \times 10^3 \text{ rad/s}$ and 26-V, 400-Hz excitation. The wheel is offset 0.20 cm in the correct direction to aid in the total pendulosity for the PIGA. The remaining pendulosity is obtained by machining a mass on one end of the float. The mass has adjusting screws for the final scale factor setting. Total pendulosity is 19.3 gm-cm.

The gas bearing operates at 10 N/cm^2 . The gas is restricted through millipore restrictors. The total flow rate of the gas bearing is $2200 \text{ cm}^3/\text{min}$. The resonant frequency of the gas bearing in the axial direction is 700 Hz; in the radial direction, it is 2000 Hz.

The angular rotation of the float is sensed by a four-pole shorted turn reluctance-type pickoff. The yoke with the four coils is mounted on the head assembly, and a bar with the shorted turns of copper is fastened to the float. The two series excitation coils are excited with 10 V at 4.8 kHz. The two series output coils have a sensitivity of 280 mV/deg. Total freedom is 0.10 rad.

Because of the limited angular rotation of the float assembly, three flexleads are used to transfer power across the gas film to the gyro. These leads are composed of 85 percent silver and 15 percent copper, and measure $5.0 \times 10^{-3} \text{ cm}$ thick by 0.015 cm wide; each has a current-carrying capability of 0.5 A (500 mA), although the gyro running current is only 135 mA and the starting current is 145 mA. They have a resonant frequency of 700 to 900 Hz when properly adjusted.

Currents for the gyro wheel and for the signal pickoff are conducted from the accelerometer housing to the head assembly by means of a miniature slipring capsule assembly. The 10 rings are 4.8 gm gold, electrodeposited over nickel and copper on an aluminum rotor. The brushes are made of gold alloy wire, bent in the shape of a "U" to contact the slipring at two diametrically opposed points. The contact resistance with the configuration is less than 0.010Ω in the bandwidth of 0 to 30 Hz at 0.10 A. The slipring assembly is mounted inside the rotor of the dc torque motor.

The servo amplifier output is applied to a direct-axis dc torque motor. It has an eight-pole, permanent-magnet stator and a 41-segment wound rotor. The commutator is designed flat to conserve space, and the commutator bars are gold-plated to prevent oxidation. Four brushes are used for redundancy,

each measuring 0.015 by 0.33 cm. The brushes are made of 50 percent silver and 50 percent graphite, and the voids are filled with molybdenum to provide lubrication and prevent arcing. Brush lead springs of like polarity have different resonant frequencies to minimize the effects of vibration upon contact resistance.

Rotation of the head assembly, which is a measure of the acceleration initially imparted to the pendulous mass, is sensed by an optical encoder. The encoder is a 14-bit incremental shaft-angle transducer. The output is a 5-V peak-to-peak sine-cosine relationship. A redundant relationship exists as a parallel output signal and is redundant back to the light source and sensors. A third output from the encoder is a zero reference signal occurring once per revolution of the measuring head. This signal is a 200-mV peak-to-peak minimum signal. The total output from the encoder is 16 384 electrical cross-overs that may be digitized to pulses.

Laboratory Test. All components utilized in making a PIGA are tested to completely evaluate the component before it is mated to a unit. This reduces time and effort in isolating trouble areas once the unit is assembled.

The evaluation and calibration of the PIGA are conducted in a one-g field, where g represents the accelerations caused by gravity at the test location. For this reason, the local gravity must be known very accurately. In practice, local gravity can be measured to $2 \times 10^{-3} \text{ cm/s}^2$. All PIGA terms are determined by positioning it at prescribed angles with respect to local gravity and measuring the component of gravity along the sensitive axis. These angles must be measured very accurately and must be repeatable in both positive and negative directions. The positioning device used, an Ultradex head, is accurate to $\pm 0.12 \mu\text{rad}$ in $\pi/180$ rad increments throughout a full 2π rad rotation.

SD-53 TEST PROGRAMS

Laboratory Calibration

The inertial sensor mounting surfaces on the SD-53 strapdown platform were qualified to an optical cube mounted on the component block. Three faces of the cube were aligned to be perpendicular to the orthogonal axes of the platform.

To evaluate the calibration and alignment of the inertial components, the platform was tested on a Goerz rate table. Each axis of the orthogonal triad was sequentially aligned along the rate table axis of rotation with the other two axes aligned perpendicular to the axis of rotation. The alignment of the platform in each position was verified with the optical cube as the reference. The calibration tests were performed while rotating the rate table with the spin axis aligned along the local vertical and also along the earth's polar axis.

The SAR gyro encoder outputs were monitored with an automatic data acquisition system (ADAS). The ADAS is built around a PDP-5 general purpose computer and three up/down counters (HP-5280A).

The ADAS was designed to operate with three independent variables: time in increments of 1 s, table angle in increments of 1.74×10^{-3} rad, and N-counts where N is an integer number of counts accumulated by a counter.

The independent variables provided an interrupt signal to the computer via the ADAS. The interrupt caused the program to log all the data provided by the ADAS.

When the program was not actively involved in logging data, it would process and print the accumulated data. The processing primarily consisted of computing the change in the dependent variable between interrupts caused by the independent variable.

When the necessary data had been acquired, they were sorted, edited, and transferred to punched cards and processed on a GE 235 computer.

The table angle was selected as the independent variable for the SAR tests and encoder pulses were the dependent variable; hence, the SAR tests have the dimensions of X counts/y radians of table rotation.

The PIGAs were calibrated with the platform mounted in three different positions on the rate table. In each test position, one axis of the platform was aligned along the rate table axis of rotation. In the PIGA tests, the Goerz rate table spin axis was aligned in the horizontal plane and pointed south. The rate table was not rotated, and the output axis of one PIGA was aligned along the local vertical. The output axes of the other two PIGAs were oriented in the horizontal plane with one PIGA pointed east and one south.

The data taken in these tests were time per head revolution. The N-count independent variable was used, where N was selected as the number of pulses per head revolution. The dependent variable in these tests was time, yielding data with dimensions of $X \mu\text{rad}/\text{one head revolution}$.

The PIGA with its sensitive or output axis vertical was checked for scale factor and bias error, while the other two PIGAs output axes were in the horizontal plane and were checked for drift errors.

To align the strapdown platform in azimuth, a porro prism was mounted on the component block and aligned with respect to the cross-range accelerometer axis. In prelaunch alignment of the strapdown platform, the azimuth will be determined by a theodolite using the porro prism as a reference.

Sled Test

The SD-53 strapdown was first integrated with the sled at Holloman Air Force Base, New Mexico, in July 1968. After laboratory test, field checks, and minor equipment modifications, tests began in February 1969. These tests were conducted primarily to prove the operational characteristics of the SD-53 in the sled environment. This is comparable to the Saturn booster or the expected space shuttle environment of linear acceleration.

Modified Saturn platform components were used on the SD-53 (AB-5 gyros and AB-3 accelerometers). The accelerometer's encoders were changed from a 600-count to a 14-bit resolution. The SARs output was an 18-bit incremental encoder. Because of the very high bit rate under thrust from the sled, the encoder outputs were recorded directly along with the necessary timing and clock reference signals. This was accomplished on three vehicle tape recorders in a redundant arrangement to overcome the response limitations of standard FM-FM telemetry. This proved to be satisfactory, as sufficient data were obtained to evaluate the test runs.

The SD-53 IMU sensor blocks were instrumented with three linear vibration transducers and three angular vibration transducers. These were mounted along the major inertial sensing axes.

Although the sled tests made with the SD-53 IMU were considered successful, several conditions prevented an accurate reduction of the test data. Some of the problems were as follows:

1. Test vehicle recorders were hard mounted. The recordings were therefore not of first quality, and the tight schedule prevented preliminary test runs with the recorders.

2. The high-SAR data rates forced operation of the recorders too close to the upper end of their bandwidth (100 Hz). The SAR data contained pulses at 25 μ s apart or 40 000 pps.

3. The data recorded via the track induction timing system were very noisy.

4. The recorder clock signal was of poor quality because of voltage drops.

5. Data calibration on the recorders did not account for such effects as electronic time delays and tape transparent skew.

6. The high resolution and frequency of the inertial sensor data created an extremely large volume of data to be processed. Programs had to be modified to allow priority of only selected intervals.

The SD-53 IMU maintained functional integrity throughout the series of sled runs where acceleration profiles ranged from 2 through 8 g linear.

A summary of the test runs is shown in Table 2. Figures 8 and 9 show the SD-53 mounted in the sled and the sled assembly.

TABLE 2. SUMMARY OF SD-53 STRAPDOWN SLED TEST

Date	Run No.	Maximum Acceleration (g)	Maximum Velocity (m/s)	Distance (m)	Run Time (s)	Mount Isolator Type
2/25/69	1	2.2	254 m	9660	91	Soft
3/4/69	2	2.2	255 m	9680	90	Soft
3/7/69	3	4.2	331 m	9790	33	Soft
3/11/69	4	8.0	350 m	-	-	Medium
3/14/69	5	7.0	431 m	9800	58	Medium

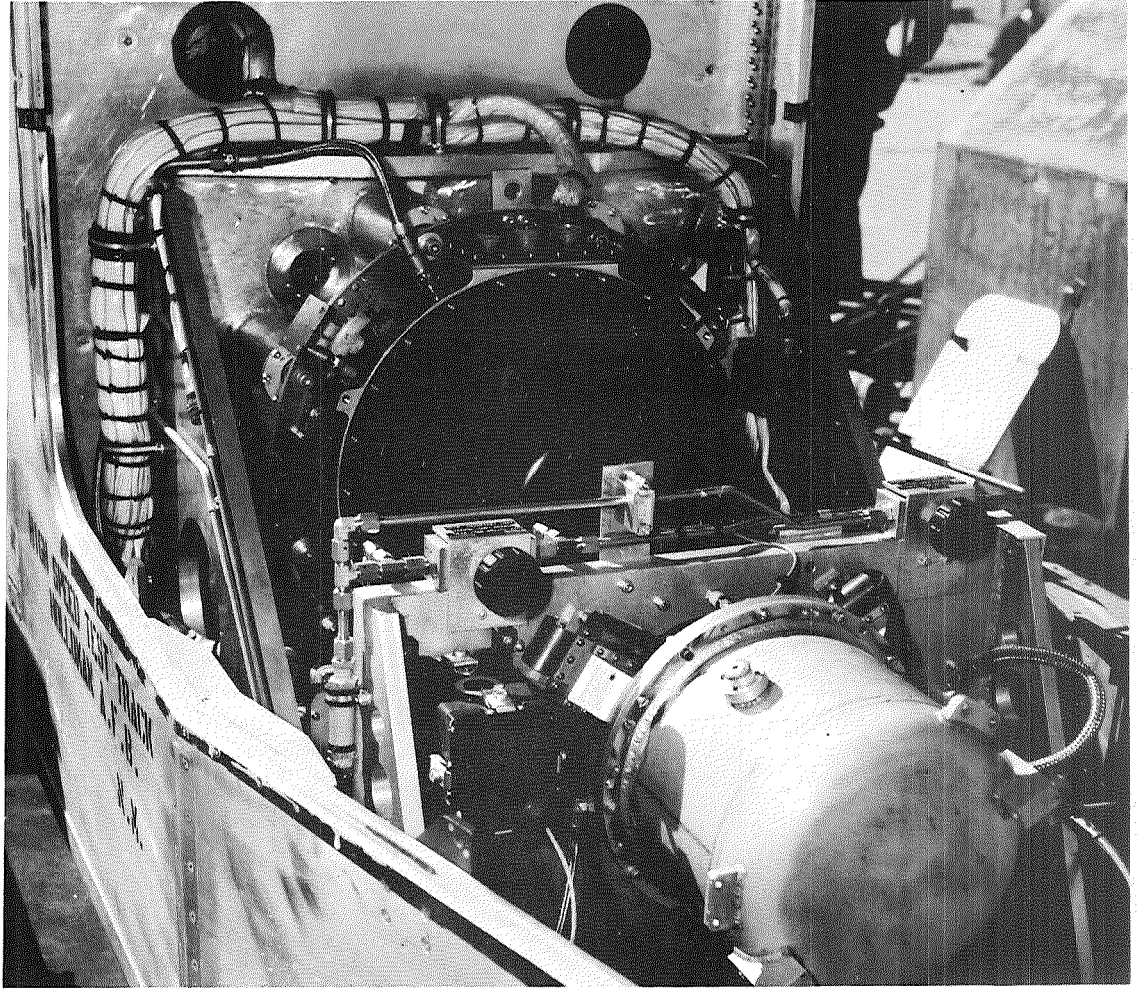


Figure 8. SD-53 installation in the sled.



Figure 9. Sled test vehicle.

Mobile Test

A truck was instrumented with the SD-53 strapdown IMU, a test console, a gas pump and supply, an SD-53 inverter, and a power supply. The strapdown component outputs were processed with a CTMC and its associated test console. Primary power was obtained from a gasoline-driven, 115-V, 45-kW generator attached to the truck with a two-wheel trailer. The truck and test equipment are shown in Figure 10.



Figure 10. Test truck installation.

The CTMC is a processor rather than a computer because it does not make logical decisions and does not contain a memory in the general sense; it can only perform addition and subtraction.

The CTMC inputs incremental sensor information, 2^{18} bits/ 2π rad from the SARs and 2^{15} bits/300 m/s from the accelerometers (PIGAs). The CTMC functional characteristics are given in Table 3.

TABLE 3. CTMC FUNCTIONAL CHARACTERISTICS

Type	Fixed-program, special-purpose digital differential analyzer, serial, fixed-point, binary.
Clock	10-MHz, 1.25-MHz bit rate, 4 clocks per bit.
Speed	39 062-Hz iteration rate, paneled word processing.
Storage	Shift registers.
Word Length	31 bits plus sign.
Input/Output	Angular rate 0.94 rad/s max. Acceleration 73g max.

The CTMC transforms the incremental outputs from the strapdown platform components into nine direction cosines and three velocities of an inertial coordinate system. A digital computer (Honeywell type DDP-516) is required to process the direction cosines to obtain the vehicle attitude and acceleration in terms of some known inertial reference system.

Identical procedures were followed in alignment of the SD-53 in the test truck before and after the test runs. The test truck is first driven into a large rotary table (10.7-m diameter) that has a positioning accuracy of $4.8 \mu\text{rad}$. With the test truck heading near north, two jacks are placed under the front bumper (one under each end). These are required to level the vehicle about the roll axis. A third jack is placed under the center of the rear bumper and is used to level the vehicle about the pitch axis. The truck is leveled to $72 \mu\text{rad}$, as readout with level indicators on the SD-53.

Figure 11 shows the SD-53 alignment in the test truck. A door on the right side (east) of the test truck is opened to expose the alignment optics on the SD-53. Theodolite 1 (T1) is positioned near the door and trained on the platform porro prism. Theodolite 2 (T2) is positioned to view both T1 and a predetermined azimuth reference (10×10 cm first surface mirror). The angle between the SD-53 and T2 is measured by T1, and T2 measures the angle between T1 and the azimuth reference. Thus, the platform azimuth is determined from these measured angles and the reference angle. The rotary table is then positioned until a north heading is achieved. The combined azimuth alignment accuracy of this alignment exercise is approximately $193 \mu\text{rad}$.

A series of three van tests was performed to test the performance of the SD-53 IMU coupled to its CTMC. These tests were performed on November 13, 19, and 20, 1970.

The basic test procedure consisted of optically aligning the IMU Y-axis along the earth's polar axis, while the X- and Z-axes were aligned to make equal angles to the local tangent plane. After the van run, the IMU axes were optically realigned to exactly the same position as described previously.

At least 0.5 hr of static prerun and 0.5 hr of static postrun data were accumulated. An event log of each run is supplied in the appendix.

The C-matrix and velocity outputs of the CTMC were recorded on seven-track IBM compatible magnetic tape. The data acquisition rate was accurately set at one scan per second. The data tapes were reduced on the UNIVAC 1108 digital computer. The quality of the magnetic tapes was excellent since only one parity record was apparent in the three reels of tapes used in the performance of the van tests.

During data reduction procedures, the raw CTMC input data were thinned by a factor of 60 to provide one data point every minute. The analysis data flow and the various coordinate frames and matrices are defined in the appendix.

All six C-matrix normalities were found to "grow" consistently as a function of time. The growth of normalities may be examined more concisely via examination of the determinant alone. Under stationary van conditions, the C-matrix determinant consistently grew at the rate of approximately 0.0013/hr. The active run produced an additional growth of about 0.002, regardless of run duration.

Determinant data are summarized in Table 4 at 15-min intervals.

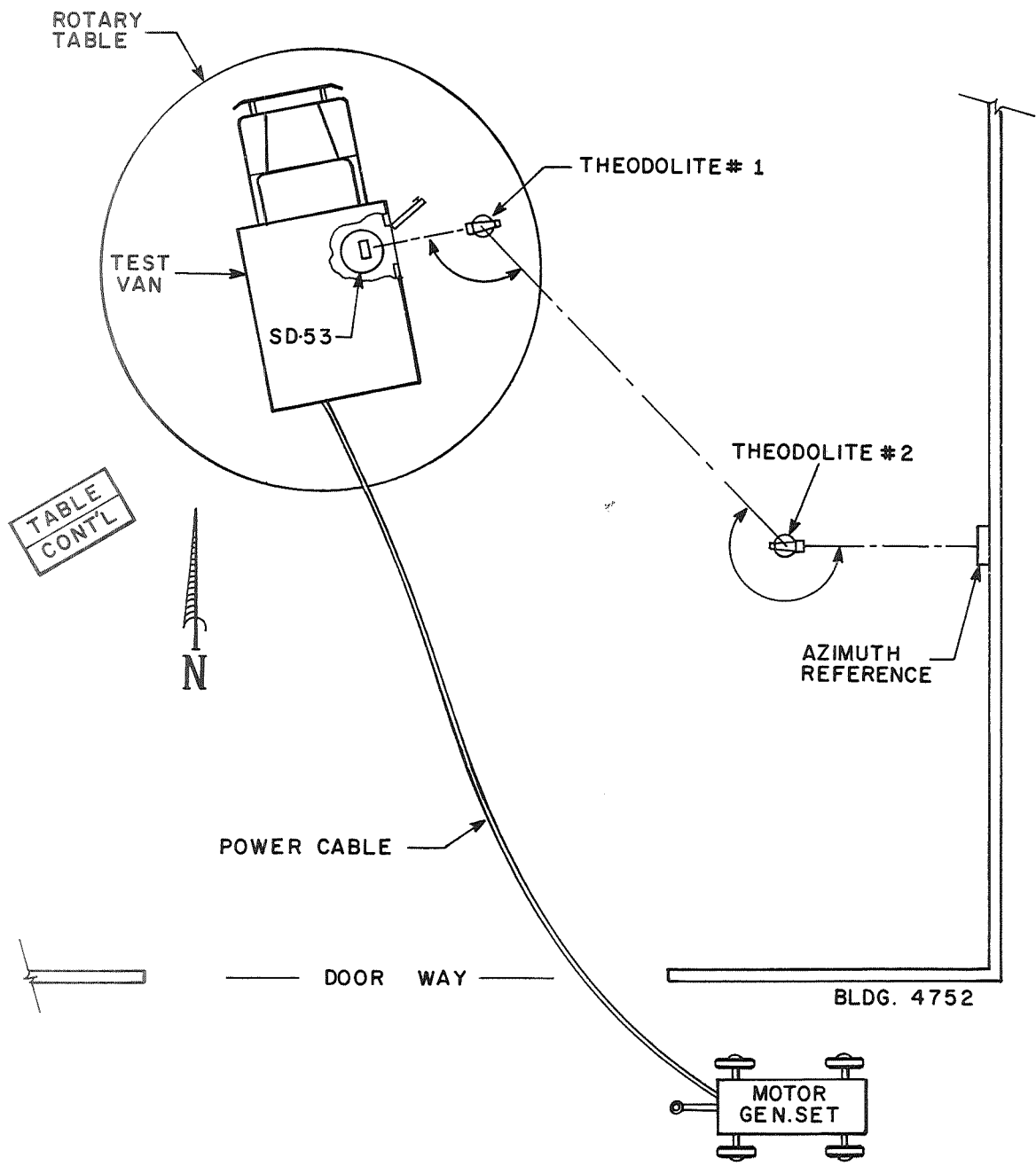


Figure 11. SD-53 alignment in test truck.

TABLE 4. DETERMINANT ERROR

Minutes	Nov. 13, 1970	Nov. 19, 1970	Nov. 20, 1970
0	0.000039	0.000012	0.000017
15	0.000340	0.000363	0.000352
30	0.000639	0.000732	0.000648
45	0.000942	0.001050	0.000987
60	0.001359	0.001366	0.002069
75	0.002310	0.001579	0.003085
90	0.003268	0.002149	0.004120
105	0.004315	0.003253	0.004455
120	0.004659	0.004256	0.004815
135	0.004988	0.005011	0.005174
150	0.005316	0.005349	0.005425
165	0.005673	0.005712	
180	0.006008	0.006052	
195	0.006325	0.006375	

ACTIVE RUN

ACTIVE RUN

ACTIVE RUN

Because the direct inertial sensor outputs were not available for analysis, the inertial axes drift rates were obtained through analysis of the CTMC C-matrix. The method used is outlined in the appendix. Results yielded rather high drift rates, but these high rates were not unexpected for the particular gyro units on the IMU block.

The approximate values of the prerun and postrun drift rates are tabulated in Table 5.

TABLE 5. INERTIAL AXES DRIFT

Date	Prerun ($\mu\text{rad/s}$)			Postrun ($\mu\text{rad/s}$)		
	X	Y	Z	X	Y	Z
11/13/70	-3.0	-10.3	-5.9	-3.9	-6.6	-4.6
11/19/70	-2.8	-8.0	-6.0	-3.7	-5.5	-4.7
11/20/70	-1.2	-6.5	-6.4	-2.6	-3.1	-5.0

The high prerun drift rates as compared to the postrun rates are probably caused by a test procedure error in the initialization of the CTMC. It was later realized that at least one initialized C-matrix set must be re-recorded for data analysis before the enablement of the IMU sensor inputs.

The change in drift rates from prerun to postrun is given in Table 6.

TABLE 6. CHANGE IN DRIFT RATE

Date	Drift Rate Change ($\mu\text{rad/s}$)		
	X	Y	Z
11/13/70	-0.97	+3.8	+1.2
11/19/70	-0.97	+1.9	+1.3
11/20/70	-1.4	+3.4	+1.4

FUTURE PLANS AND PROGRAMS

Dodecahedron SAR Strapdown IMU and Computer

Design has begun on two dodecahedron SAR strapdown IMUs. The first will be considered a breadboard and is designated DDH-BB (Fig. 12). The second will be an accurately machined frame and is designated DDH-MKI (Fig. 13).

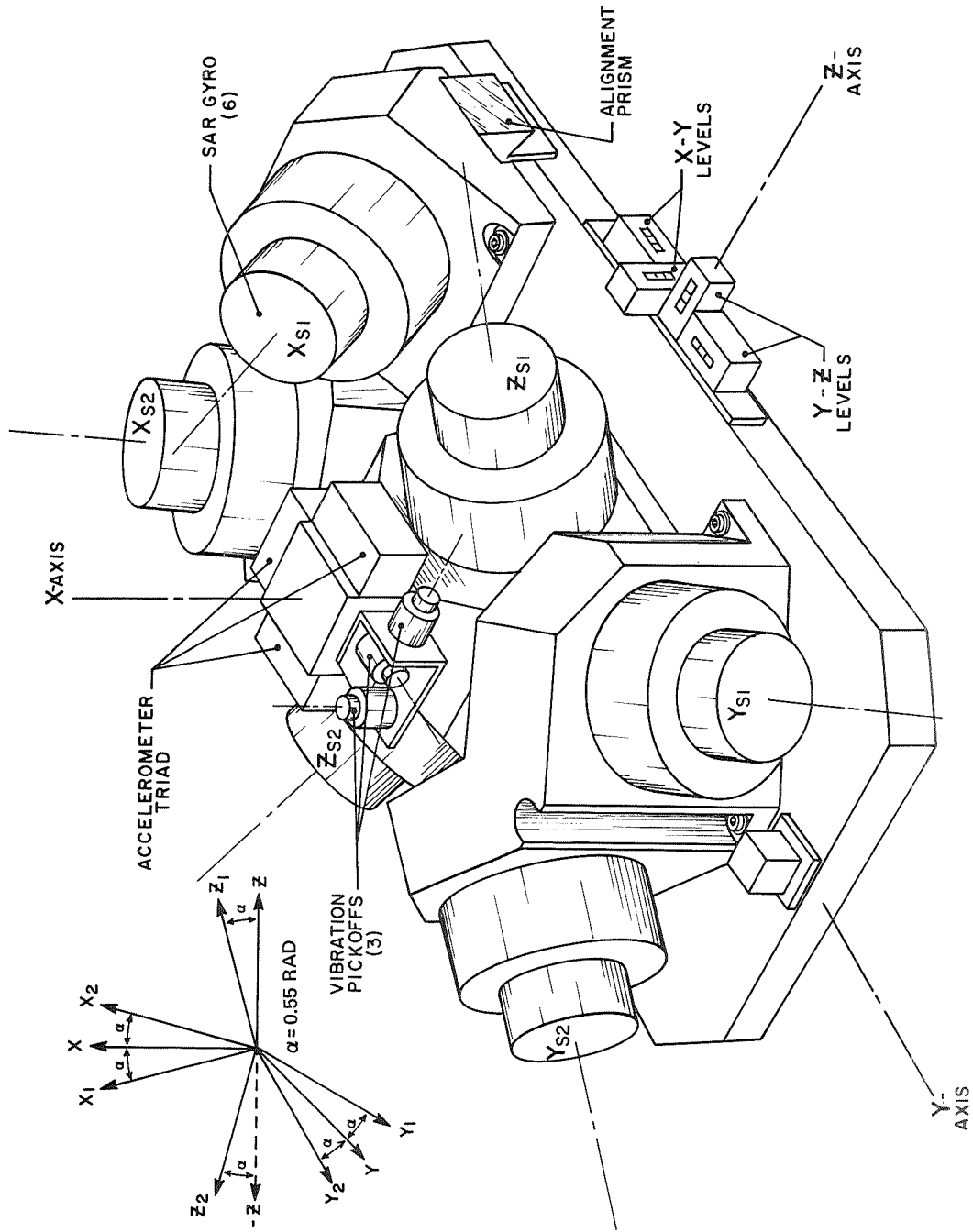


Figure 12. Breadboard SAR strapdown IMU.

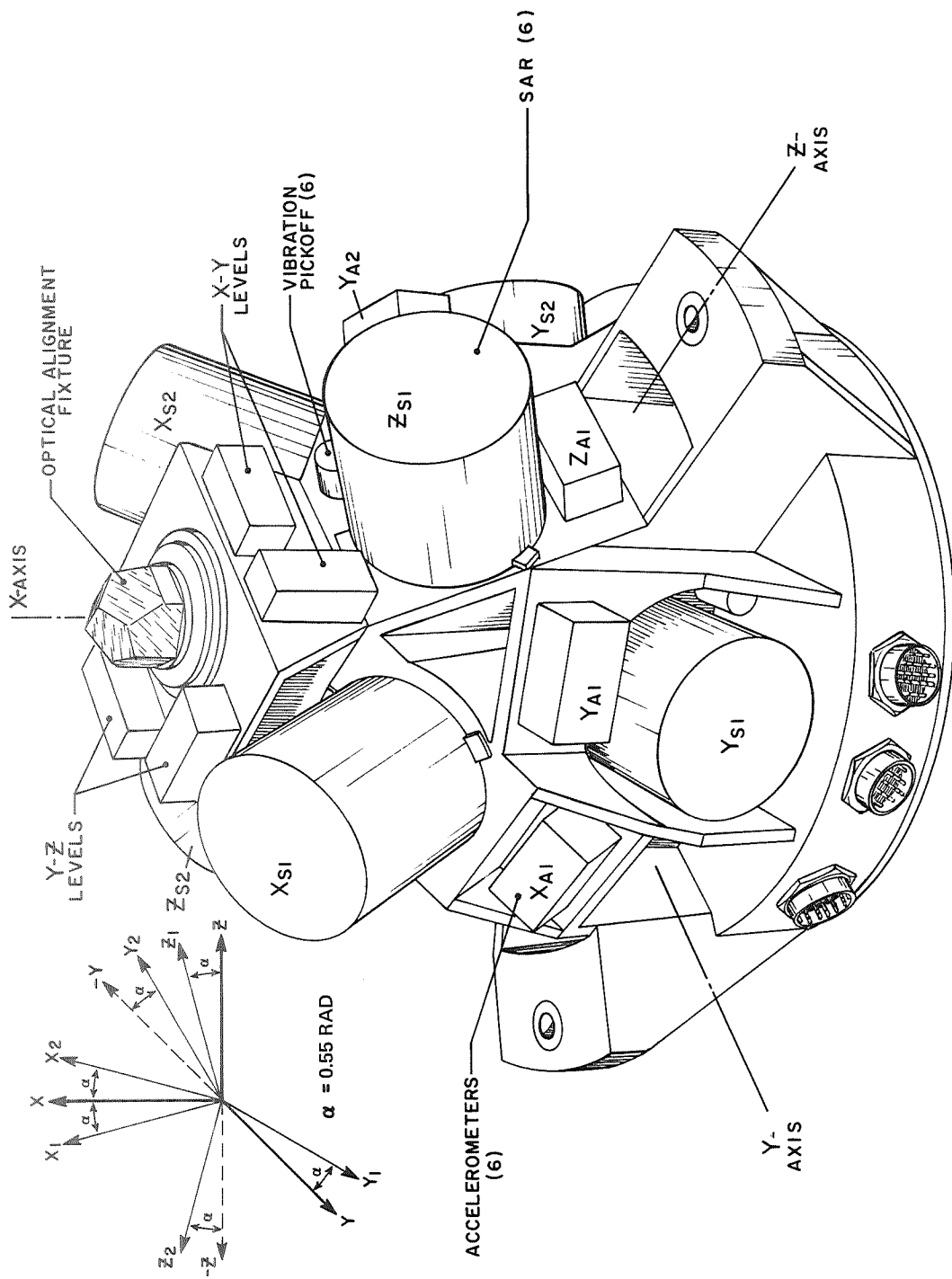


Figure 13. DDH-MKI SAR strapdown IMU.

These redundant SAR strapdown IMUs will be tested and evaluated in the laboratory and in the field. Mobile field tests will be run with a specially equipped test van to determine the integrity of the IMUs. Together with the computer support equipment, the IMUs will furnish attitude and navigation information. It is also proposed that further field tests will be performed in an airplane and, if possible, tests will be made aboard a space booster vehicle to evaluate the redundant IMU system under flight environmental conditions.

The DDH-BB contains five or six refurbished AB-5 air bearing SARs and a triad of Kearfott 2401 force balance-type accelerometers mounted on a 45×61 -cm aluminum plate. The electronics is mounted in a separate box above the components and provides the system cable interface to power, computer, and checkout console. The DDH-BB contains pressure and thermal sensors to control the gyro gas bearing supply and preheaters. A triad of vibration accelerometers is provided to evaluate environmental conditions. In addition, levels, an optical cable, and a prism are provided for alignment aids.

The electronic box is rigidly mounted to the base plate to provide a simple cable interface to the outside systems and test console. This is necessary because of limited slings available on the Goerz test stand in the laboratory. Most of the cable harness between the electronics and breadboard will be pigtail connectors to simplify the wiring and minimize cable lengths. The electronic box contains servo amplifiers, relays, power supplies, digital logic interface circuits, and servo pulsing circuits. It also has circuits and components to create faults in the system to exercise failure detection, isolation, and evaluation. The 400-Hz inverter and 4.8-kHz power systems are external to the box and are incorporated in the test equipment.

The DDH-MKI strapdown IMU consists of a mounting frame machined in a dodecahedron configuration. There are two line replaceable units (LRU); one consists of an SAR (with Kearfott Alpha III gyros), its servoloop, power supply, control and monitoring circuits, and encoder electronics. The other LRU consists of a 2401 forced balanced accelerometer, its servoloop, and the digital output circuits.

The vibration pickoffs and alignment optics are mounted independently from the LRUs. There are six SARs and six accelerometer LRUs. The input axes of the SARs that are common to the same plane are skewed to achieve the angle of 2α (0.55 rad). The LRUs each have independent cable and connector interface.

The servo electronics and control logic will be high-density integrated circuits.

Both SAR strapdown IMUs will be evaluated together with a Honeywell DDP-516 computer and its input and output peripheral equipment. The computer was obtained in a ruggedized version to withstand the environment of a test van or airplane. A complete list of the DDP-516 characteristics is given in Table 7.

TABLE 7. HONEYWELL DDP-516 COMPUTER CHARACTERISTICS

Type	Parallel binary
Addressing	Single address with indexing and indirect addressing
Word length	16 bits
Machine code	2s complement
Memory type	Magnetic core
Memory size	4096
Memory cycle time	0.96 μ s
Speed	Add and subtract 1.92 μ s
Multiply	5.28 μ s (max)
Divide	10.56 μ s (max)
Peripheral equipment	ASR — 33 teletype unit with the following: Reads, punches, and types at 10 characters per second Keyboard input Off-line paper — tape preparation, reproduction, and listing
Other accessory equipment	Magnetic tape 6 up/down counters, 12-bit stationary binary Real-time clock (Honeywell 316/516/12) Frequency — 60 Hz incremented every 10 ms

New Gyro Considerations

The performance of any inertial guidance system depends upon the characteristics and functions exhibited by the basic inertial components, e. g., the gyros and accelerometers. The fundamental gyro requirements are accuracy, stability, reliability, repeatability, low weight, low power, and modest cost. Many types of components are being pursued as candidates for the future IMUs. Among these are the liquid bearing gyro and the laser gyro (Figs. 14 and 15).

The liquid bearing gyro (LB-5) is a logical extension of the gyro technology as related to the hydrostatic output axis suspension designs. A number of inertial instruments that employ this type of output axis suspension have been designed; however, all of these have been gas bearings. The requirements for future applications indicate that the gas bearing would have certain disadvantages. This design pursues the hydrostatic output axis suspension but with a fluid rather than gas. This type of suspension is desirable because it does not require pivots, jewels, or magnetic induced forces to support the gyro gimbal. The decision to pursue the LB-5 gyro has also been influenced because a noncompressible fluid can be pumped more efficiently than a gas. For the three prototype instruments on Contract No. NAS8-24414, no changes were made in the piece parts normally assembled in the Saturn V AB-5-K8 gyro that would change any parameter of the gas bearing. This permits testing of the assembly as a gas bearing instrument before filling it with the fluid. It also permits establishing techniques for insuring the cleanliness of the bearing to an extremely high degree of accuracy.

The three liquid bearing gyros have been on test at MSFC since March 1970. Some gyro tests at temperatures of 25° to 45°C have resulted in a mean of 0.29 $\mu\text{rad/s}$ with a 1 σ of 0.058 $\mu\text{rad/s}$, with the same gyro temperature stabilized to around the 45°C operating point. The mean remained at 0.29 $\mu\text{rad/s}$ with a 1 σ of 0.0015 $\mu\text{rad/s}$. These tests have been conducted primarily to investigate the stability and magnitude of the bias terms of the liquid bearing. The results of these tests indicate that the performance of the three gyros has been equivalent to that of the Saturn gas bearing, and these gyros are adaptable to SAR IMUs.

Laser gyros have been under development by several contractors and MSFC contracts. The ring laser inertial sensor, developed by the Sperry Rand Corporation, is a multiple-beam interferometer which, when rotated about an axis normal to its plane, converts optical phase shifts into optical frequency differences. Two highly coherent and oppositely traveling light

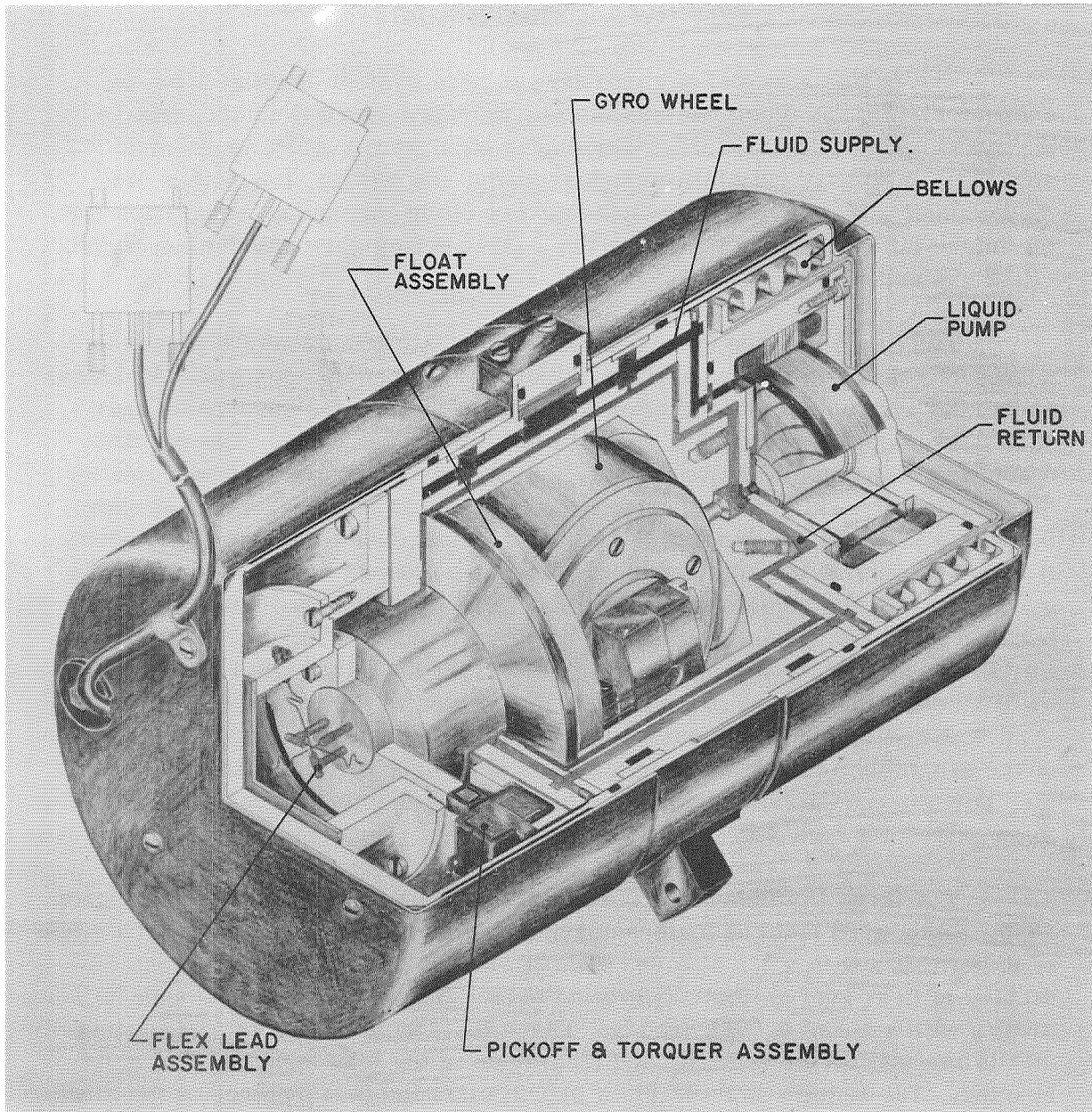


Figure 14. Liquid bearing gyro: LB-5.

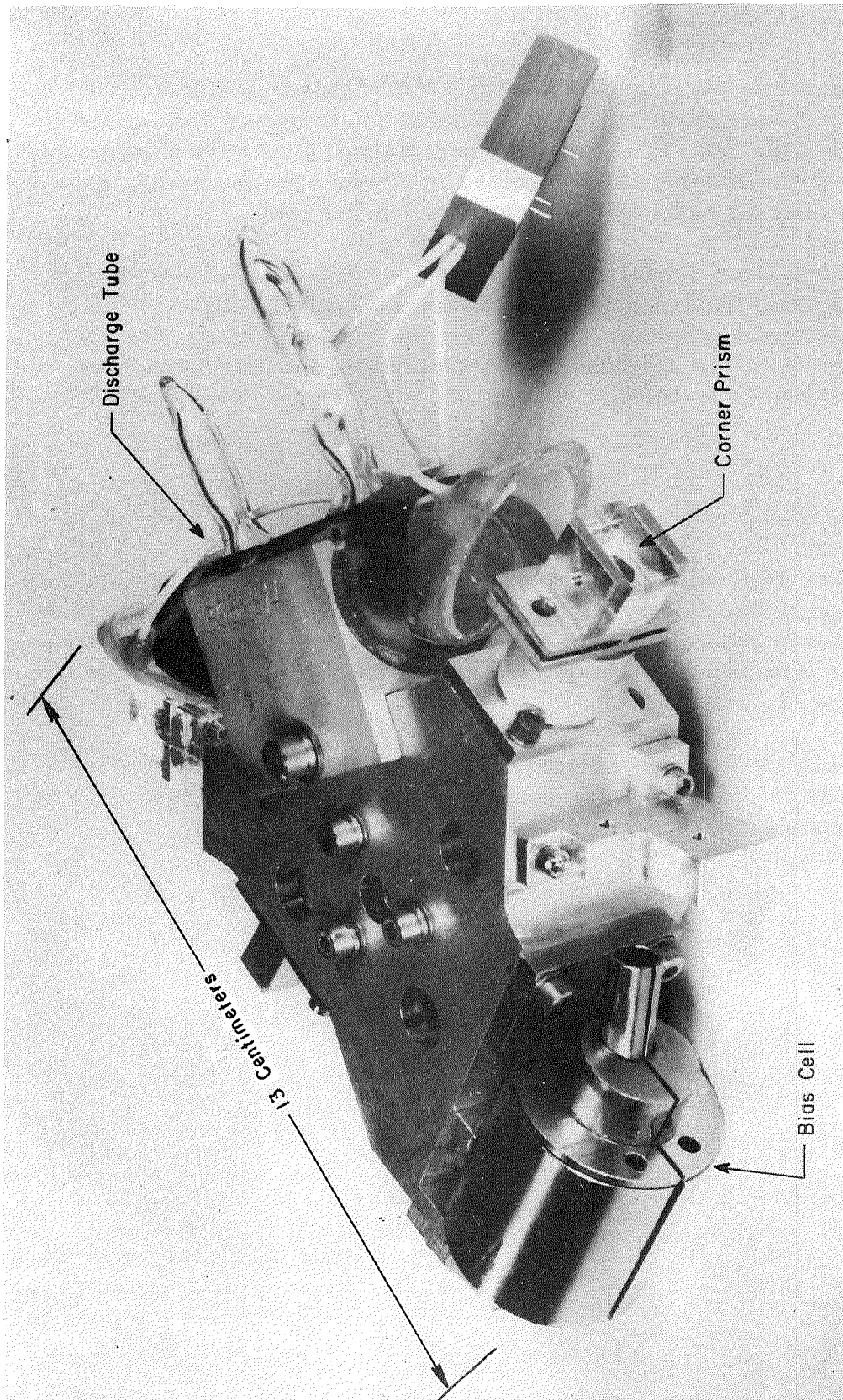


Figure 15. Single-axis ring laser gyro.

waves are generated by laser action along a closed path, which forms the required laser resonant cavity. Rotation alters the frequency (or, inversely wavelength) of the light. The frequency is decreased for a wave propagating in the direction of rotation and is increased for a wave in the opposite direction. Frequency alteration is proportional to rotation rate.

The ring laser sensor has now progressed past the laboratory device stage. At present performance levels, the ring appears ideally suited to a number of aerospace systems. Specifically, its dynamic range, linearity, angular resolution, and ruggedness mean that it need not be isolated from angular motions of the vehicle.

CONCLUSION

Theory and laboratory and field testing have demonstrated that the SAR IMU provides distinct advantages over the conventional strapdown IMU. The development and testing of the SD-53 have evolved into a prototype and flight design dodecahedron SAR IMU. These systems are now scheduled for development, testing, and evaluation.

With the development of high quality and new inertial sensors, the redundant SAR IMU could become a formidable candidate for the space shuttle guidance system.

APPENDIX

THE EVENT LOG, COORDINATE DESCRIPTION, AND DRIFT RATE COMPUTATIONS FOR COMPUTER REDUCTION

Tables A-1 through A-3 denote the event logs of procedures followed to evaluate the SD-53/CTMC strapdown platform system during the mobile van test. The data flow diagram is shown in Figure A-1. Table A-4 denotes the coordinate frames and the matrix equations developed to evaluate the SD-53/CTMC performance characteristics.

TABLE A-1. SD-53/CTMC VAN TEST: NOVEMBER 13, 1970,
EVENT LOG

Real Time	Event	Lapsed Minutes
11:00	Enable SD-53	0
11:47	Turn table	47
12:03	Connect generator cart	63
12:05	Turn onto Martin Road	65
12:09	Turn onto Rideout Road	69
12:17	Turn onto Goss Road	79
12:33	Turn onto Martin Road	93
12:39	Stop at Rideout Road	99
12:42	Turn to building	102
12:45	On rotary table	105
13:45	Aligned	165
14:15	Stopped	195

TABLE A-2. SD-53/CTMC VAN TEST: NOVEMBER 19, 1970,
EVENT LOG

Real Time	Event	Lapsed Minutes
07:57	Begin test	0
09:15	Remove jacks	78
09:19	Rotate table	82
09:21	Begin backing truck	84
09:24	Connect generator cart	87
09:26	Move out	89
09:30	Martin and Rideout Roads	93
09:39	Goss Road	102
09:45	Patton Road	108
09:54	Martin Road	117
10:00	Rideout and Martin	123
10:02	Parking lot	125
10:07	On rotary table	130
10:53	Aligned	176
11:26	End test	209

TABLE A-3. SD-53/CTMC VAN TEST: NOVEMBER 20, 1970,
EVENT LOG

Real Time	Event	Lapsed Minutes
11:35	Begin test	0
12:20	Remove jacks	45
12:21	Move table	46
12:23	Back off table	48
12:25	Connect generator cart	50
12:28	Turn onto Martin Road	53
12:29	Martin and Rideout Roads	54
12:36	Begin loop to Patton Road	61
12:38	Railroad on Patton Road	63
12:43	Patton gate	68
12:45	Goss Road	70
12:51	Rideout Road	76
13:00	Martin Road	85
13:01	Turn off Martin Road	86
13:02	In parking area	87
13:04	On rotary table	89
13:43	Aligned	128
14:15	End test	160

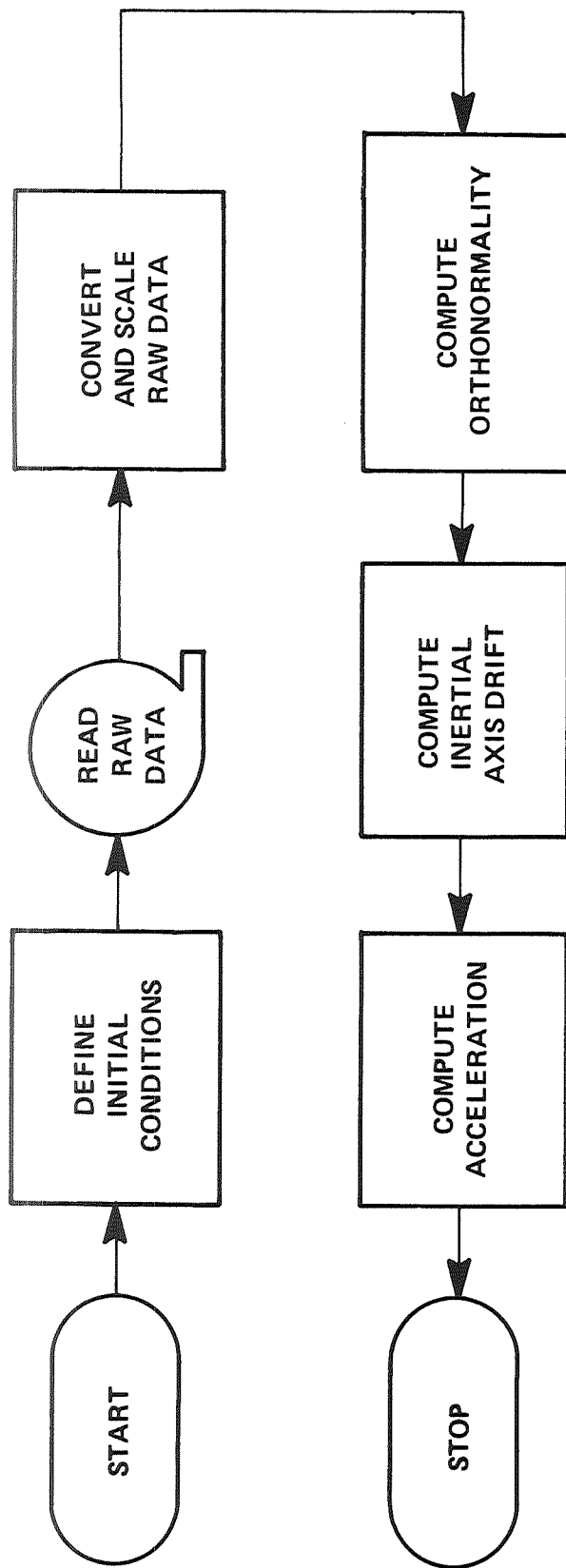
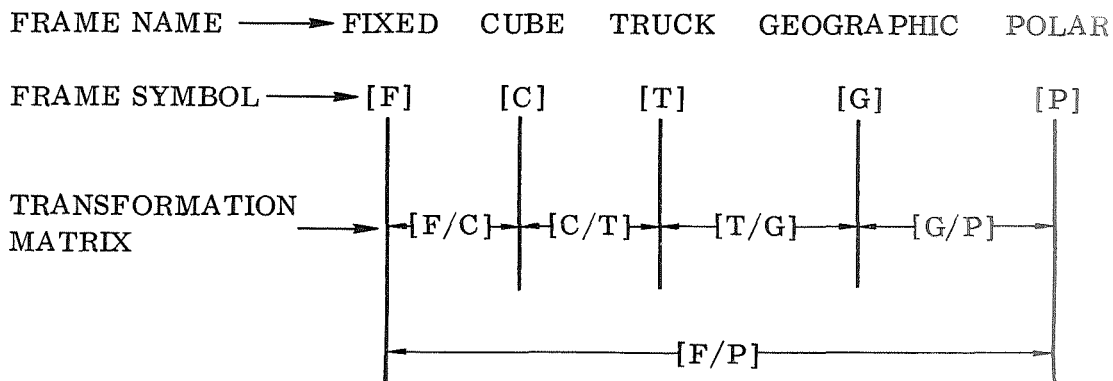


Figure A-1. Simplified data reduction flow.

TABLE A-4. VAN TEST COORDINATES FRAMES



Frame Definitions

Symbol	Frame Name	Unit Vectors		
		X-Axis	Y-Axis	Z-Axis
[F]	Inertially fixed	Inertial X	Inertial Y	Inertial Z
[C]	Optical cube	Red cube face	Yellow cube face	Blue cube face
[T]	Truck (test van)	Truck roll	Truck pitch	Truck yaw
[G]	Geographical	North	West	Vertical up
[P]	Polar	Pseudo-east	Polar north	Meridian plane

[F/C] MATRIX

The [F/C] matrix is the output of the CTMC. It is considered a function of time and devoted by:

$$[F/C] = \begin{bmatrix} C_{11} & C_{12} & C_{13} \\ C_{21} & C_{22} & C_{23} \\ C_{31} & C_{32} & C_{33} \end{bmatrix} .$$

[C/T] MATRIX

The [C/T] matrix reflects the manner in which the IMU is mounted in the truck. This matrix actually reflects the placement of the IMU optical cube to a porro prism mounted on the IMU base plate. This matrix is considered constant and is defined by:

$$[C/T] = \begin{bmatrix} -1/\sqrt{2} \sin \lambda & -1/\sqrt{2} & 1/\sqrt{2} \cos \lambda \\ \cos \lambda & 0 & \sin \lambda \\ -1/\sqrt{2} \sin \lambda & 1/\sqrt{2} & 1/\sqrt{2} \cos \lambda \end{bmatrix} ,$$

where λ is the local astronomical latitude.

[T/G] MATRIX

For both the prerun and postrun data reduction, the [T/G] matrix is taken as the identity matrix; e. g.:

$$[T/G] = \begin{bmatrix} 1 & 0 & 0 \\ 0 & 1 & 0 \\ 0 & 0 & 1 \end{bmatrix} .$$

[G/P] MATRIX

The [G/P] matrix is considered constant and is defined by:

$$[G/P] = \begin{bmatrix} 0 & \cos \lambda & -\sin \lambda \\ -1 & 0 & 0 \\ 0 & \sin \lambda & \cos \lambda \end{bmatrix} .$$

[F/P] MATRIX

The [F/P] matrix reflects the earth's polar rate and is defined by:

$$[F/P] = \begin{bmatrix} \cos (\omega T + \pi/4) & 0 & \sin (\omega T + \pi/4) \\ 0 & 1 & 0 \\ -\sin (\omega T + \pi/4) & 0 & \cos (\omega T + \pi/4) \end{bmatrix} .$$

where

ω = polar earth rate (rad/s).

T = lapsed time from IMU sensor input enable (s).

NOTE: The initial bias $\pi/4$ is necessary to force the initial [F/C] and [T/G] matrices to be the identity matrix.

INERTIAL AXES DRIFT DEFINITION

Using the basic rules of matrix multiplication yields:

$$[F/P] = [F/C][C/T][T/G][G/P] .$$

The $[F/P]$ error matrix $[\epsilon_{F/P}]$ should be defined so that

$$[F/P] = [\epsilon_{F/P}][F/P]_N \quad ,$$

where $[F/P]_N$ is the nominal (ideal) fixed to polar matrix.

Solving the above equations and recalling that $[F/P]_N$ is orthonormal yields:

$$[\epsilon_{F/P}] = [F/C][C/T][T/G][G/P][F/P]_N^T \quad .$$

Under the prerun and postrun conditions of no van motion, the $[T/G]$ matrix may be considered constant (and more precisely, the identity matrix). Since both the $[C/T]$ and $[G/P]$ matrices were defined as constant, the $[C/P]$ matrix may be precalculated as

$$[C/P] = [C/T][T/G][G/P] \quad .$$

The error matrix may now be expressed as

$$[\epsilon_{F/P}] = [F/C][C/T][F/P]_N^T \quad .$$

Now if the inertial axes drift is assumed "small," it can be defined as

$$[\epsilon_{F/P}] = \begin{bmatrix} 1 & \zeta_z & -\zeta_y \\ -\zeta_z & 1 & \zeta_x \\ \delta_y & -\delta_x & 1 \end{bmatrix} = \begin{bmatrix} \epsilon_{11} & \epsilon_{12} & \epsilon_{13} \\ \epsilon_{21} & \epsilon_{22} & \epsilon_{23} \\ \epsilon_{31} & \epsilon_{32} & \epsilon_{33} \end{bmatrix} \quad .$$

It can then be concluded that the inertial axes drift at time T from IMU sensor enable time T_0 may be expressed as

$$\omega_x \approx \frac{\epsilon_{23} - \epsilon_{32}}{2T}$$

$$\omega_y \approx \frac{\epsilon_{31} - \epsilon_{13}}{2T}$$

$$\omega_z \approx \frac{\epsilon_{12} - \epsilon_{21}}{2T}$$

under the conditions that

$$\epsilon_{11} \approx 1$$

$$\epsilon_{22} \approx 1$$

$$\epsilon_{33} \approx 1$$

$$\epsilon_{12} \approx -\epsilon_{21}$$

$$\epsilon_{13} \approx -\epsilon_{31}$$

$$\epsilon_{23} \approx -\epsilon_{32}$$

BIBLIOGRAPHY

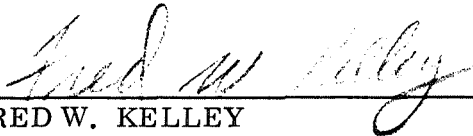
Gismondi, T., and T. Armstrong: A Description of the Single-Axis Reference Rate Sensor. Sperry Rand Report No. SP-208-0423, October 30, 1970.

SINGLE-AXIS REFERENCE STRAPDOWN
INERTIAL MEASURING UNIT

By Charles E. Lee

The information in this report has been reviewed for security classification. Review of any information concerning Department of Defense or Atomic Energy Commission programs has been made by the MSFC Security Classification Officer. This report, in its entirety, has been determined to be unclassified.

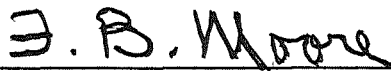
This document has also been reviewed and approved for technical accuracy.



FRED W. KELLEY
Chief, Integration and Flight Qualification Branch



CARL H. MANDEL
Chief, Guidance and Control Division



F. B. MOORE
Director, Astrionics Laboratory

DISTRIBUTION

NASA TM X-64586

INTERNAL

DIR
DEP-T
AD-S
A&TS-MS-H
A&TS-MS-IL (8)
A&TS-MS-IP (2)

A&TS-PAT
Mr. L. D. Wofford, Jr.

A&TS-TU
Mr. Winslow (15)

PD-DO-DIR
Dr. Thomason

S&E-CSE-DIR
Dr. Haeussermann

S&E-ASTR-DIR
Mr. Moore
Mr. Horton
Mr. Powell

S&E-ASTR-S
Mr. Wojtalik
Mr. Brooks

S&E-ASTR-C
Mr. Swearingen
Mr. Bridges
Mr. Garrett

S&E-ASTR-G
Mr. Mandel
Dr. Doane
Mr. Jones
Mr. Doran
Mr. Broussard
Mr. Morgan

Mr. Fikes
Mr. Walls
Mr. Gaines
Mr. Clark
Mr. Kalange
Mr. Caudle
Mr. Wood
Mr. Kelley
Mr. Lee (20)
Mr. Cook
Mr. Grubb
Mr. Sims

S&E-ASTR-A
Mr. Hosenthien
Miss Flowers

PM-PR-M

EXTERNAL

National Aeronautics and Space
Administration
Washington, D. C. 20546
Attn: Mr. R. C. Livingston, MTG
Mr. T. S. Michaels, REG

Scientific and Technical Information
Facility (25)
P. O. Box 33
College Park, Maryland 20740
Attn: NASA Representative (S-AK/RKT)